International Journal of Thermodynamics (IJoT)
ISSN 1301-9724 / e-ISSN 2146-1511
www.ijoticat.com

Vol. 23 (No. 1), pp. 1-11, 2020
doi: 10.5541/ijot.633485
Published online: Mar 01, 2020

Optimal Condition of Finite Number of Heat-Recovery Cycles for a Non-Isothermal Heat Source

Keisuke Takeshita*, Yoshiharu Amano

WISE, Waseda University, Tokyo, Japan
E-mail: take@power.mech.waseda.ac.jp, yoshiha@waseda.jp

Received 15 October 2019, Revised 2 December 2019, Accepted 2 December 2019

Abstract

This study analyzes a temperature condition that produces maximal power from a non-isothermal heat source under a finite number of heat-recovery thermodynamic cycles. Some previous studies have theoretically analyzed a system utilizing thermal energy from heat sources under multiple thermodynamic cycles assuming a constant heat-source temperature. However, many heat sources for heat-recovery thermodynamic cycles are non-isothermal, where the temperature changes considerably during heat exchange with the cycles. Therefore, it is necessary to consider the temperature change of the heat source. First, a condition that maximizes the power generated by a combination of single/multiple Carnot cycles from constant-specific-heat heat sources is analyzed, and the optimal temperature is derived analytically. Subsequently, simulations of the Rankine cycle and several patterns of the Kalina cycle are compared with those of the analytical model. These comparisons reveal that the proposed model effectively estimates the condition for heat-recovery cycles that produce maximal power from a non-isothermal heat source. Using the proposed method, the required number of cycles and their operating conditions under a given heat source condition are estimated, without any information about cycle configurations, types of working fluids, and iteration of simulation calculation under inappropriate conditions. In addition, a systematic exploration of the optimal system can be started from the proper initial condition.

Keywords: *Rankine cycle; Kalina cycle; Optimization; Maximal power; Non-isothermal heat source.*

1. Introduction

From the viewpoint of sustainability, energy sources are being shifted from fossil fuels to renewable/unused energies. Representatives of these energy sources are wind, solar, geothermal, waste heat, and solar thermal energies, of which the latter three are primarily middle- to low-temperature heat sources.

Currently, power generation from middle- to low-temperature heat sources constitutes a low market share because of the low cost of primary energy. However, fossil fuel reserves are finite; therefore, the value of these heat sources will increase once the fossil fuel reserves are exhausted.

Middle- to low-temperature heat sources are typically consumed where they are generated and primarily converted into three types of energy forms: power, heat, and cooling. Necessary forms of these three types are designed to be produced at a plant on the site (such as a power plant, combined heat and power, or combined cooling, heat, and power). They are conventionally composed of multiple thermodynamic cycles under a single high-temperature heat source.

Among the heat-recovery cycles, the organic Rankine cycle (ORC), Kalina cycle (KC), and absorption heat pump cycles (AHP) are the most feasible and have been extensively studied [1-7]. Compared to AHP, ORC and KC exhibit high flexibility in terms of configuration and operating conditions; therefore, different configurations of cycles and working fluids are proposed for various environmental conditions [8-18]. Walraven et al. [4] investigated the performances of a KC and three configurations of ORC, and optimized them for 100–150 °C geothermal heat sources. Various configurations, including subcritical, transcritical, multipressure, recuperation, and turbine bleeding, and up to 80 different working fluids, were considered. They concluded that transcritical and multipressure subcritical ORCs are the best performing cycles (in most cases) and outperform the investigated KC at low-heat-source outlet temperatures. Dai et al. [8] optimized subcritical ORCs, both with and without a recuperator, for 10 different working fluids using a genetic algorithm. The working fluid R236EA demonstrated the highest exergy efficiency under a 145 °C heat source, and the recuperator was not always useful. Hettiarachchi et al. [14] examined the performance of a KC for low-temperature geothermal heat sources and compared it with that of an ORC. The performance was considered in terms of the heat-exchange area per unit power produced, and the KC exhibited a better overall performance than the ORC at moderate pressures.

Previous studies have demonstrated that cycle performance and operating conditions can be estimated for different cycle configurations and working fluids and that they differ for various environmental conditions. Therefore, in the system-design stage, different possibilities of various working fluids, cycle configurations, and operating conditions should be considered. However, it is not practical to execute simulations for all these scenarios. Estimations of cycle performance and operating conditions using limited parameters (such as heat-source temperature) will significantly assist system-design processes.

*Corresponding Author

A few studies have analyzed systems that utilize thermal energy from a heat source under multiple thermodynamic cycles in a cascade. For example, Bejan [19] analyzed a "combined-cycle power plant" under the condition of a constant total thermal conductance. They concluded that when the total heat-exchange inventory is fixed and the design is optimized for maximal power, the plants are characterized by the Chambadal–Novikov–Curzon–Ahlborn [20] efficiency. The analysis assumed a constant heat-source temperature, such as that in the gas turbine cycle, whose heat source temperature can be regarded as approximately constant. However, many heat sources for heat-recovery thermodynamic cycles are non-isothermal, where the temperature changes considerably during heat exchange with the cycles.

Therefore, an analysis that considers the temperature gradient of the heat source is necessary. In addition, the difference between the analysis and actual cycles must be evaluated. To this end, the study makes the following contributions:

- Analysis of the condition that maximizes the output power of finite thermodynamic cycles from a single non-isothermal high-temperature heat source.
- Comparison between sufficiently optimized ORC/KC simulations and the analytical model under the same environmental conditions.

2. Analysis

For a non-isothermal heat source, maximal power can be produced by a succession of many infinitesimal reversible power-producing compartments [21]. Conversely, developing excessive cycles results in heat dissipation. Therefore, in practical situations, the minimum number of cycles has an advantage. Thus, it is important to investigate the relations among the number of cycles, operating conditions, and performance.

In this study, an analytical model that involves a single or succession of multiple Carnot cycles (CCs) under constant (including infinite)-specific-heat heat sources (hot source (HS) and cold source (CS)) is developed. Figure 1(a) shows a case in which the number of cycles is three. An individual CC receives heat from a HS at temperature $T_{\mathrm{HS},i}$ and produces power, W_i. The HS is cooled down to temperature $T_{\mathrm{HS},i+1}$, and the minimum temperature differences between the cycle and heat sources are $\Delta T_{\mathrm{a},i}$ and $\Delta T_{\mathrm{b},i}$, respectively, as shown in Figure 1(b). HS is cooled down to temperature $T_{\mathrm{HS,ext}}$ after it exits the final cycle, and the heat that cannot be utilized by the cycles is assumed to dissipate to the ambient air.

The heat transferred from HS, $\dot{Q}_i$, and the power produced by a cycle, W_i, are defined as follows:

$$\dot{Q}_i = c_{\mathrm{HS}}\dot{m}_{\mathrm{HS}}\left(T_{\mathrm{HS},i} - T_{\mathrm{HS},i+1}\right), \tag{1}$$

$$W_i = \dot{Q}_i\left(1 - \frac{T_{\mathrm{l},i}}{T_{\mathrm{h},i}}\right). \tag{2}$$

The condition for maximal power is as follows:

$$\frac{d\sum_{j=i}^{n} W_j}{dT_{\mathrm{h},i}} = 0 \quad (\text{for } i = 1 \text{ to } n), \tag{3}$$

where n is the number of CCs.

The exergy efficiency, ε_n, is defined as follows:

$$\varepsilon_n = \frac{W_{\mathrm{sum}}}{c_{\mathrm{HS}}\dot{m}_{\mathrm{HS}}e_{\mathrm{HS},1}} = \frac{\sum_{j=1}^{n} W_j}{c_{\mathrm{HS}}\dot{m}_{\mathrm{HS}}\left(T_{\mathrm{HS},1} - T_0 - T_0 ln\left(\frac{T_{\mathrm{HS},1}}{T_0}\right)\right)}, \tag{4}$$

where T_0 is the ambient temperature.

2.1 Zero Temperature-Difference Condition

The simplest analysis is in the case where the minimum temperature differences between the cycles and heat sources are zero. This condition is expressed as follows:

$$\Delta T_{\mathrm{a},i} = \Delta T_{\mathrm{b},i} = 0. \tag{5}$$

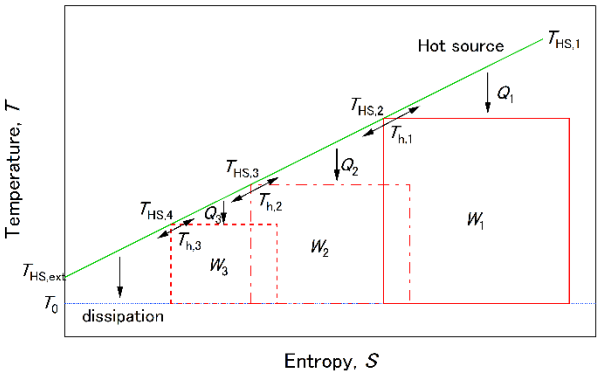

(a) Three-cycle arrangement

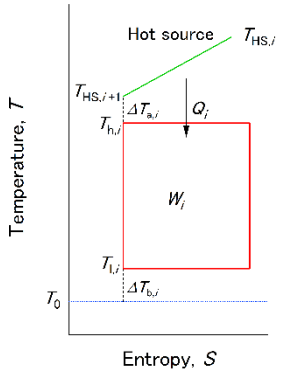

(b) Decomposed single cycle

Figure 1. Succession of three CCs arranged under a constant-specific-heat HS.

2.1.1 Exit HS Temperature Equals Ambient Temperature

Next, the case in which the exit HS temperature, $T_{\mathrm{HS,ext}}$, equals the ambient temperature, T_0, is considered. This condition is expressed as follows:

$$T_{\mathrm{HS,ext}} = T_0. \tag{6}$$

(a) Single cycle

When the number of cycles is one, the condition for maximal power, from Eq. (3), is expressed as follows:

$$T_{\mathrm{h},1} = \sqrt{T_{\mathrm{HS}1}T_0} = T_0(T_{\mathrm{HS}1}/T_0)^{\frac{1}{2}}. \tag{7}$$

(b) Two cycles

The conditions for maximal power by two cycles are as follows:

$$T_{\mathrm{h},1} = T_0\left(T_{\mathrm{HS},1}/T_0\right)^{\frac{2}{3}},\ T_{\mathrm{h},2} = T_0\left(T_{\mathrm{HS},1}/T_0\right)^{\frac{1}{3}}. \tag{8}$$

(c) Three cycles

The conditions for maximal power by three cycles are as follows:

$$T_{\mathrm{h},1} = T_0\left(T_{\mathrm{HS},1}/T_0\right)^{\frac{3}{4}},\quad T_{\mathrm{h},2} = T_0(T_{\mathrm{HS}1}/T_0)^{\frac{1}{2}},$$
$$T_{\mathrm{h},3} = T_0\left(T_{\mathrm{HS},1}/T_0\right)^{\frac{1}{4}}. \tag{9}$$

From Eqs. (7)–(9), when the number of cycles is n, the high-temperature of each cycle, $T_{\mathrm{h},i}$, can be expressed as follows:

$$T_{\mathrm{h},i} = T_0\left(T_{\mathrm{HS},1}/T_0\right)^{\frac{n-i+1}{n+1}}. \tag{10}$$

Eq. (10) indicates that the ratios of cycle-1 inlet HS temperature, $T_{\mathrm{HS},1}$, the high-temperature of each cycle, $T_{\mathrm{h},i}$, and ambient temperature, T_0, are constant. Eq. (8) is obtained by utilizing Eq. (7), and similarly, Eq. (8) leads to Eq. (9); therefore, it is estimated that Eq. (10) will be fulfilled when the number of cycles, n, is greater than four.

Figure 2 shows the exergy efficiency, ε_n, when the ambient temperature, T_0, is assumed to be 25 °C. The efficiency, ε_n, increases slightly and monotonically when $T_{\mathrm{HS},1}$ increases. The limits of ε_1, ε_2, and ε_3 as $T_{\mathrm{HS},1}$ approaches T_0 (=25 °C) are 1/2, 2/3, and 3/4, respectively. They correspond to the left ends of the curves, and minimum value of the exergy efficiency in each number of cycles, n. This indicates that the limit of ε_n becomes $1 - 1/(n+1)$. Therefore, number of the cycles should be selected as it satisfies the required exergy efficiency, ε_n.

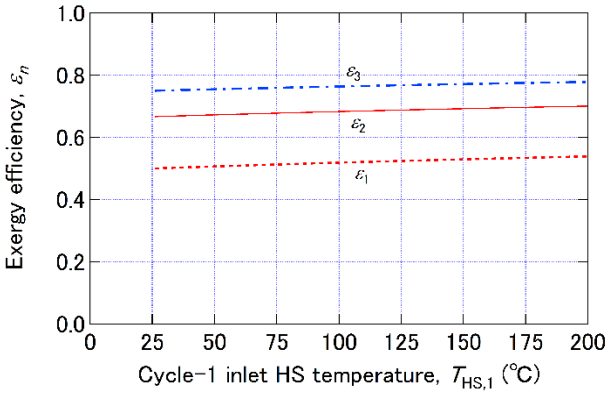

Figure 2. Efficiencies when exit HS temperature equals the ambient temperature.

2.1.2 Effect of Exit HS Temperature

When the exit HS temperature varies, the temperature condition for maximal power changes. The turning point is the high-temperature of the last cycle, $T_{\mathrm{h},n}$, under the assumption that the exit HS temperature, $T_{\mathrm{HS,ext}}$, equals the ambient temperature, T_0 (i.e., the results in section 2.1.1.).

(a) Lower Exit HS Temperature

When the exit HS temperature, $T_{\mathrm{HS,ext}}$, is lower than $T_{\mathrm{h},n}\big|_{T_{\mathrm{HS,ext}}=T_0}$, the result becomes the same as in section 2.1.1., because $T_{\mathrm{HS,ext}}$ does not restrict $T_{\mathrm{h},n}$.

$$T_{\mathrm{h},i} = T_0\left(T_{\mathrm{HS},1}/T_0\right)^{\frac{n-i+1}{n+1}}\Big|_{T_{\mathrm{HS,ext}}\le T_0\left(T_{\mathrm{HS},1}/T_0\right)^{\frac{1}{n+1}}}. \tag{11}$$

(b) Higher Exit HS Temperature

When the exit HS temperature, $T_{\mathrm{HS,ext}}$, is higher than $T_{\mathrm{h},n}\big|_{T_{\mathrm{HS,ext}}=T_0}$, the high-temperature of the final cycle, $T_{\mathrm{h},n}$, equals $T_{\mathrm{HS,ext}}$. In this case, $T_{\mathrm{h},n}$ is fixed, and the optimization process becomes equivalent to that examined by the remaining cycles. Figure 3 shows an example where the number of cycles is three. Here, both cycle-1 and cycle-2 are divided into equivalent cycles, indicated as thick broken-line red squares. Any lateral succession of CC arrangement as that shown in Figure 1(a) has an equivalent longitudinal CC arrangement similar to that shown in Figure 3.

$$T_{\mathrm{h},i} = T_{\mathrm{HS,ext}}\left(T_{\mathrm{HS},1}/T_{\mathrm{HS,ext}}\right)^{\frac{n-i}{n}}\Big|_{T_{\mathrm{HS,ext}}\ge T_0\left(T_{\mathrm{HS},1}/T_0\right)^{\frac{1}{n+1}}}. \tag{12}$$

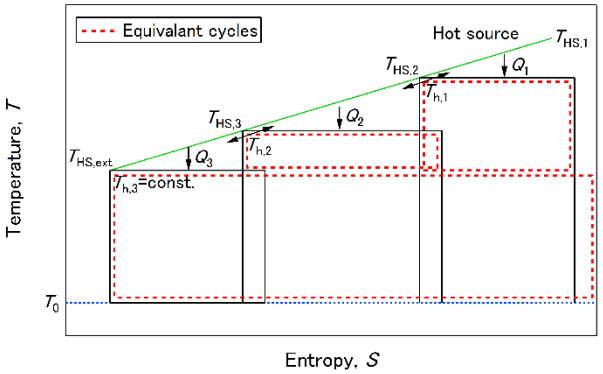

Figure 3. High exit HS temperature condition (and equivalent arrangement).

2.2 More Practical Condition

In the case where $\Delta T_{\mathrm{a},i}$ and $\Delta T_{\mathrm{b},i}$ are realistic values, Eq. (3) should be similarly solved to maximize the output power. The result can be expressed concisely when $\Delta T_{\mathrm{a},i}$ and $\Delta T_{\mathrm{b},i}$ are constant.

$$\begin{cases} T_{\mathrm{h},i} = T_\beta\left(T_\alpha/T_\beta\right)^{\frac{n-i+1}{n+1}}\Big|_{T_\gamma\le T_\beta\left(T_\alpha/T_\beta\right)^{\frac{1}{n+1}}} \\ T_{\mathrm{h},i} = T_\gamma\left(T_\alpha/T_\gamma\right)^{\frac{n-i}{n}}\Big|_{T_\gamma\ge T_\beta\left(T_\alpha/T_\beta\right)^{\frac{1}{n+1}},} \end{cases} \tag{13}$$

where $T_\alpha = T_{\mathrm{HS},1} - \Delta T_{\mathrm{a}}$, $T_\beta = T_0 + \Delta T_{\mathrm{b}}$, and $T_\gamma = T_{\mathrm{HS,ext}} - \Delta T_{\mathrm{a}}$.

3. Discussion

In this section, the results obtained using the CC model (in section 2) are compared with those obtained using the optimized Rankine cycle (RC) and KC. A KC is a modified RC that uses an ammonia–water mixture (AWM) as the working fluid. For comparison, ammonia and AWM are chosen as the working fluids for RCs (ammonia Rankine cycle (ARC) and AWM Rankine cycle (AWMRC), respectively). The parameters affected by the model (temperature, exergy efficiency, and net output power) are expressed as CC estimation (CCE).

Figures 4 and 5 show schematic diagrams of the single RC and KC, respectively. AWMRC is included in the KC because it is equivalent to a KC with constraint conditions. Both the RC and KC comprise four primary components: an evaporator (EV), condenser (CON), turbine (TB), and pump (PM). Other auxiliary components include high- and low-temperature recuperators (HR and LR, respectively), separator, preheater (PH), and superheater (SH).

Henceforth, the numbering subscripts of parameters, such as state quantities, correspond to the numbers in Figures 4 and 5 (e.g., $T_{\mathrm{HS},1}$) unless specified otherwise.

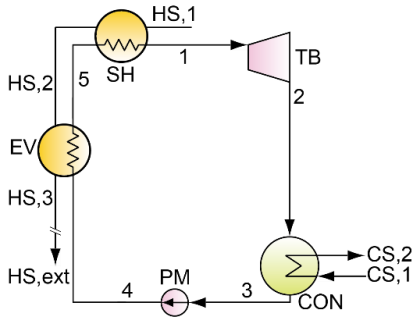

Figure 4. Schematic diagram of the single ARC.

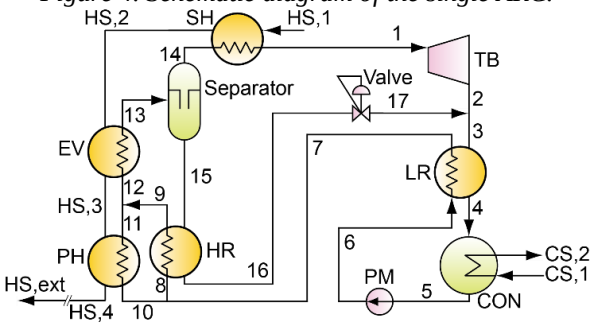

Figure 5. Schematic diagram of the single KC.

3.1 Modeling, Simulation Tools, and Algorithm

Thermodynamic models are developed based on mass and energy balances. For simplicity and comparison with the CC model, the models involve the following assumptions:

- HS and CS are constant (including infinite)-specific-heat fluids.
- All components are under ideal conditions (no heat dissipation; no pressure losses; no kinetic and potential energy variations; ideal counterflow heat exchangers; and dry saturated vapor or saturated liquid at the outlets of several components)
- Throttling at the expansion valves is isenthalpic.
- The pumping and expansion processes are isentropic, and the minimum temperature differences at each heat exchanger are zero, unless specified otherwise.

A simulation program is written in FORTRAN using PROPATH version 13.1 [22]. The thermodynamic properties of ammonia and AWM are based on the formulations proposed by Tillner–Roth et al. [23] and Ibrahim and Klein [24], respectively. The cycle-operating conditions are obtained using a convergence calculation. An enumerative method with a heuristic is employed for searching the maximum output power.

Table 1 shows the input parameters for single cycles. The input parameters for the program include the pressures, temperatures, ammonia mass fraction, mass flow rate (ratio), efficiencies, and pinch temperatures of the heat exchangers. The variables P_{D} and x_{13} indicate the dewing pressure and dryness fraction at the EV outlet, respectively.

Table 1. Input parameters for single cycles.

Cycle type	ARC	KC	AWMRC
Input parameters (Common)	T_1, $T_{\mathrm{HS},1}$, $T_{\mathrm{HS,ext}}$, $T_{\mathrm{CS},1}$, $T_{\mathrm{CS},2}$, η_{TB}, η_{PM}, $\Delta T_{\mathrm{p,EV}}$, $\Delta T_{\mathrm{p,SH}}$, $\Delta T_{\mathrm{p,CON}}$, $c_{\mathrm{HS}} = 1$ [kJ/(kg K)]		
Input parameters (Individual)	P_1, $\dot{m}_{\mathrm{HS}}$	P_{13}, T_{13}, z_6, $\dot{m}_8$, $\Delta T_{\mathrm{p,HR}}$, $\Delta T_{\mathrm{p,LR}}$, $\Delta T_{\mathrm{p,PH}}$, $\dot{m}_6$(or $\dot{m}_{\mathrm{HS}}$)	
Conditions to be noticed			$P_{13} < P_{\mathrm{D}}$, $x_{13} = 1$

3.2 Parameters for Cycle Performance

Exergy efficiency, ε, is defined as the ratio of net output power to the exergy of HS at the inlet of cycle-1:

$$\varepsilon = \frac{W_{\mathrm{net}}}{\dot{m}_{\mathrm{HS}} e_{\mathrm{HS},1}}. \quad (14)$$

The thermal efficiency, η_{thm}, is defined as the ratio of the net output power to the heating rate at the evaporator:

$$\eta_{\mathrm{thm}} = W_{\mathrm{net}} / \dot{Q}_{\mathrm{EV}}. \quad (15)$$

3.3 Comparison with RC

The simulation program of the ARC can calculate multicycle arrangement. The cycles are numbered in the order of higher evaporating temperature. If the parameters of the cycle corresponding to the cycle number must be distinguished, then the number will be added to the end of the numbering subscripts of the parameters (e.g., $T_{\mathrm{HS},3,i}$).

The EV-outlet HS temperature of the i-th cycle, $T_{\mathrm{HS},3,i}$, becomes the SH inlet temperature of the next cycle, $T_{\mathrm{HS},1,i+1}$.

3.3.1 Optimization and Error Analysis

Figure 6 shows flowcharts of ARC simulation in the case where the number of the cycles is two. There are three hierarchies: A, B, and C; B utilizes A, and C utilizes B. The conservation laws and temperature differences between the heat sources and ARC are satisfied in hierarchy A. The maximum net power of the single cycle is searched by changing the evaporating pressure, $P_{1,i}$, in hierarchy B. In hierarchy C, cycle-1 and -2 are calculated in a cascade, and the sum of the net powers, W_{sum}, is maximized by changing the intermediate HS temperature. ΔW and $\Delta T_{\mathrm{HS,ext},i}$ express the differences in the net power and HS exit temperature between a loop and the 1-time previous loop.

In this study, the working fluid is assumed to be maximally superheated at SH. Neglecting the error in the calculation of the thermodynamic properties, errors can occur by each iteration loop. The errors are estimated to be within 0.00025 K for temperature, 50 Pa for pressure, and 0.035 % for power, W_{sum}.

3.3.2 Validation

The thermodynamic model of RC in this study and the optimization method are simultaneously validated by comparing a calculation result with that of an optimized single ARC by Dai et al. [8]. The input conditions correspond to case A-1 in Table 2. Table 3 compares the results and shows that the model in this study agrees well with Dai's model. The 0.07 MPa higher evaporating pressure, P_1, is derived by the calculation in this study, and the thermal efficiency becomes 0.03 % higher than the Dai's result.

Table 2. Input conditions for ARC simulation.

Case	A-1	A-2	A-3
N	1	2	2
P_1 [MPa]	Optimal		
T_1 [°C]	135	Maximum	
$T_{\mathrm{HS},1,1}$ [°C]	145	50-150 (2-K-step)	100
$T_{\mathrm{HS,ext}}$ [°C]	20	25	26-98 (2-K-step)
$T_{\mathrm{CS},1}(=T_{\mathrm{CS},2})$ [°C]	20	25	25
η_{TB}	0.85	1	1
η_{PM}	0.6	1	1
$\Delta T_{\mathrm{p,EV}}$ [K]	8	0	0

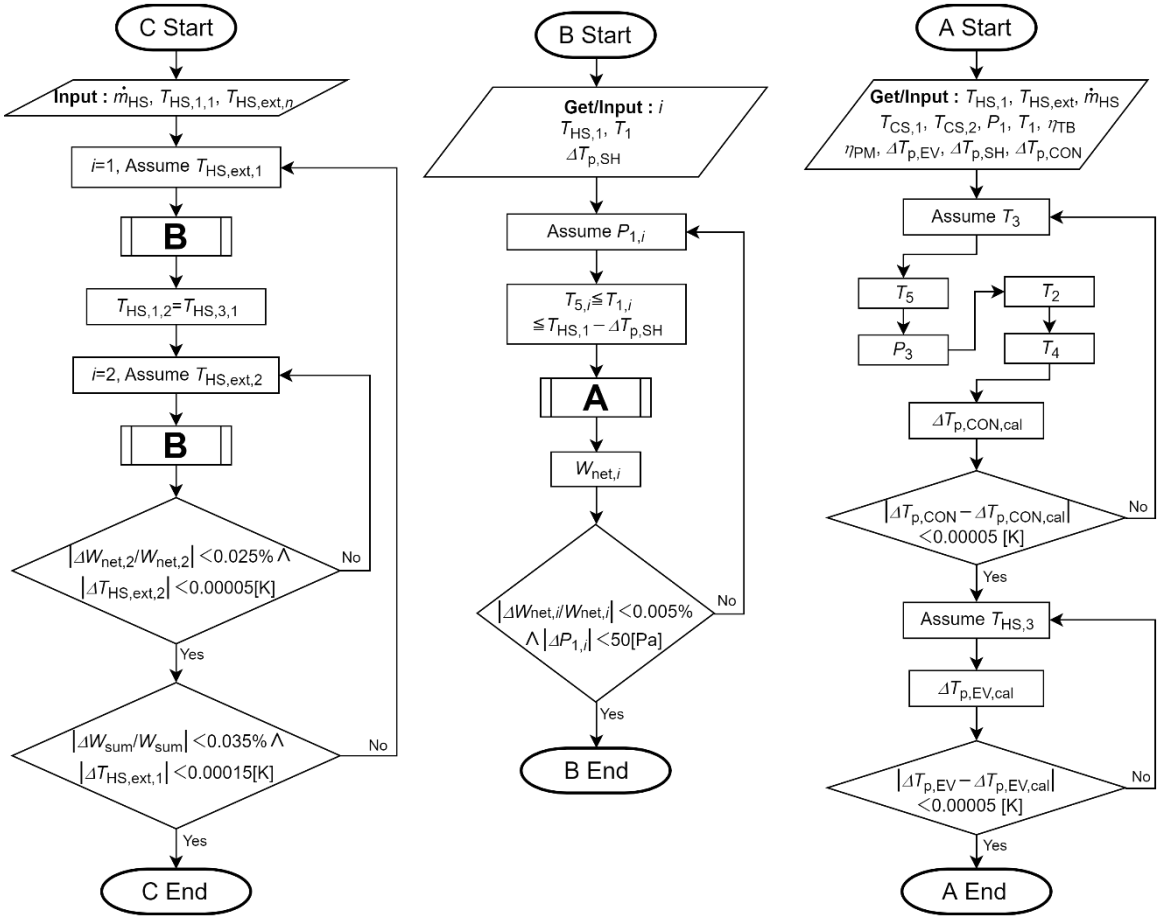

$\Delta T_{p,CON}$ [K]	5	0	0

Table 3. Validation of ARC model with Dai's results.

Case	Dai [8]	A-1
$T_{HS,3}$ [°C]	71.15	71.44
P_1 [MPa]	3.90	3.917
P_3 [MPa]	1.003	1.003
T_4 [°C]	26.43	26.44
η_{thm} [%]	12.10	12.13

3.3.3 Effect of Cycle-1 Inlet HS Temperature

Similarly, as shown in section 2.1.1., the effect of cycle-1's inlet HS temperature, $T_{HS,1,1}$, is investigated. The input conditions correspond to case A-2 of Table 2.

The evaporating temperature, $T_{5,i}$, and exergy efficiency, ε_2, when $T_{HS,1,1}$ is changed are shown in Figure 7 (a) and (b), respectively. The thick broken lines and thin solid lines indicate RC and CCE, respectively. The estimation shows good agreement with $T_{5,1}$, while differences in $T_{5,2}$ and ε_2 increase with $T_{HS,1,1}$.

This is due to the difference in heating process between the RC and CC; that is, the temperature profile of the heating process of ammonia allows cycle-1 (RC-1) to utilize HS with a lower temperature than the estimated temperature, and the cycle-2 (RC-2) inlet HS temperature becomes lower than the estimated temperature. Therefore, the heat ratio of RC-1, $\frac{\dot{Q}_{EV,1}+\dot{Q}_{SH,1}}{(\dot{Q}_{EV,1}+\dot{Q}_{SH,1})+(\dot{Q}_{EV,2}+\dot{Q}_{SH,2})}$, increases and the total exergy efficiency approaches that of RC-1.

In addition, the reducing degrees of RC-1 outlet HS temperature increases with $T_{HS,1,1}$, because the evaporation latent heat decreases with an increase in the evaporating pressure. Consequently, the differences between RC and CCE in the cycle-2 evaporating temperature, $T_{5,2}$, and exergy efficiency, ε_2, increase with $T_{HS,1,1}$.

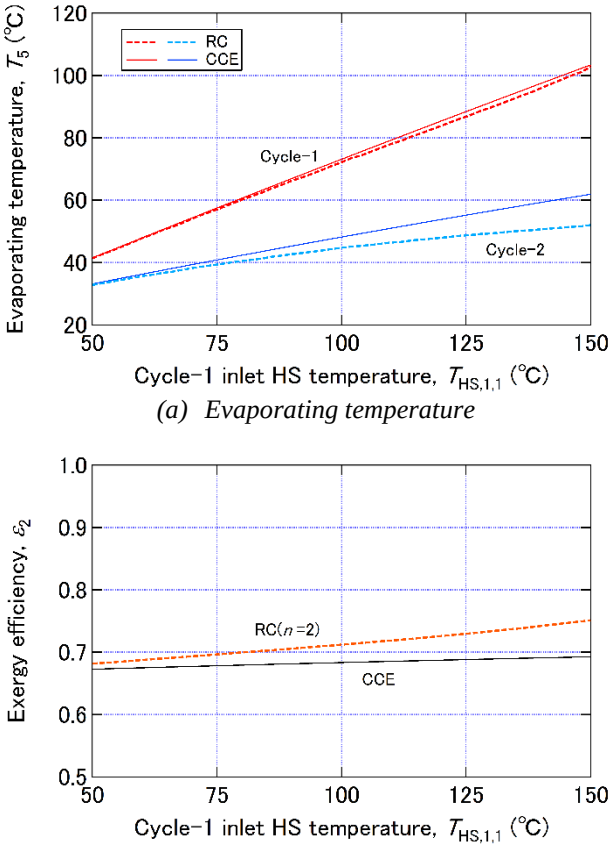

(a) Evaporating temperature

(b) Exergy efficiency

Figure 7. Effect of cycle-1 inlet HS temperature.

3.3.4 Effect of Exit HS temperature

Similarly, as shown in section 2.1.2., the effect of $T_{\mathrm{HS,ext}}$ is investigated. The input conditions correspond to case A-3 of Table 2.

The evaporating temperatures, $T_{5,i}$, and exergy efficiency, ε_2, when $T_{\mathrm{HS,ext}}$ is changed are illustrated in Figure 8 (a) and (b), respectively. The meanings of the lines are the same as Figure 7. The findings indicate that both the temperatures, $T_{5,i}$, and estimated temperatures exhibit similar trends for each cycle. Both $T_{5,i}$ are higher than the estimated temperatures by approximately 2 K in the range above 48 °C for each cycle; hence, RC-2 is not applicable at temperatures above 74 °C. The efficiency, ε_2, is higher than the estimated value by approximately 4.2 % in the range below 48 °C, and increases with $T_{\mathrm{HS,ext}}$.

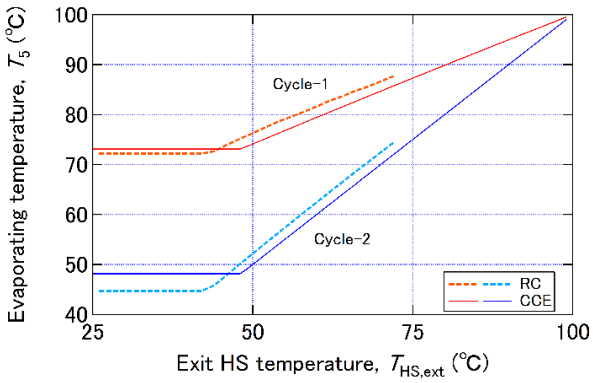

(a) Evaporating temperature

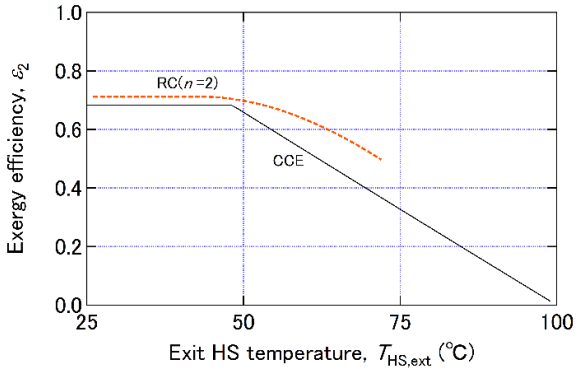

(b) Exergy efficiency

Figure 8. Effect of exit HS temperature.

3.3.5 Output Power of Two Cycles

The sum of the net powers is investigated when n is two. It is considered that the difference between CCE and the RC simulation typically appears in this condition.

The input conditions correspond to those shown in Table 4; that is, the cycle-1 outlet HS temperature ($T_{\mathrm{HS,3,1}}$ for RCs and $T_{\mathrm{HS,2}}$ for CCs) varies as a parametric input. Figure 9 shows the sum of the net powers per unit HS, W_{sum}, to the cycle-1 outlet HS temperature.

The maximum power of RCs is 5.77 kW/(kg s^{-1}) at 67 °C $T_{\mathrm{HS,3,1}}$, and that of CCE is 5.53 kW/(kg s^{-1}) at 73 °C $T_{\mathrm{HS,2}}$. The difference between them is 6 K in the temperature and 4% in the power.

Table 4. Parametric input of cycle-1 outlet HS temperature.

Case	**A-4**	
Cycle No.	1	2
P_1 **[MPa]**	Optimal	
T_1 **[°C]**	Maximum	
$T_{\mathrm{HS,1}}$ **[°C]**	100	$T_{\mathrm{HS,3,1}}$ (RC) / $T_{\mathrm{HS,2}}$(CC)
$T_{\mathrm{HS,ext}}$ **[°C]**	40-90 (1-K-step)	25
$T_{\mathrm{CS,1}}(=T_{\mathrm{CS,2}})$ **[°C]**	25	25
$\Delta T_{\mathrm{p,EV}}$ **[K]**	0	
$\Delta T_{\mathrm{p,CON}}$ **[K]**	0	

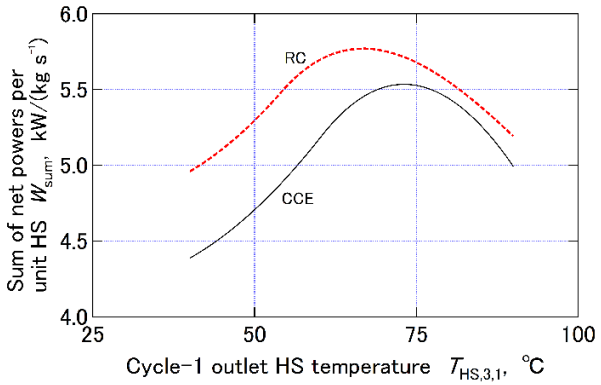

Figure 9. Parametric input of cycle-1 outlet HS temperature.

3.4 Comparison with KC

3.4.1 Optimization and Error Analysis

The flowcharts of the KC simulation are illustrated in

ırts of ARC simulation.

Figure 10. There are three hierarchies: A, B, and C; B utilizes A, and C utilizes B. The conservation laws and temperature differences at the heat exchangers are satisfied in hierarchies A and B, respectively.

In hierarchy C, the evaporating pressure, P_1, EV outlet temperature, T_{13}, EV inlet mass fraction, z_6, SH outlet temperature, T_1, and HR mass flow rate (ratio), $\dot{m}_8$, are optimized with respect to the net power. Among these parameters, z_6 is regarded as a parametric input, and the temperature, T_{13}, is converted to the dryness fraction at the EV outlet, x_{13}, before hierarchy B is started.

The parameters to be optimized are changed alternately. Each time, a parameter is searched as it yields the local maximum of the output power, and the parameter changes are iterated until the net power becomes convergent. The exergy efficiency is evaluated as an objective function because the EV mass flow rate, $\dot{m}_6$, is inputted as a constant and the net power cannot be directly compared. $\Delta\varepsilon$, ΔP_{13}, Δx_{13}, ΔT_1, and $\Delta\dot{m}_8$ express the differences between a loop and the 1-time previous loop.

Neglecting the error in the calculation of the thermodynamic properties, errors can occur by each iteration loop and calculation of pinch temperatures. Pinch temperatures are calculated as the minimum temperature differences among the 1/1280 equally divided sections with respect to enthalpy change. Because the sum of the temperature differences of the cycle is considered approximately the same as that between SH inlet HS and CON inlet CS, the sum of the errors obtained by the calculations of the pinch temperatures is estimated to be within 150/1280 K. Therefore, the errors are estimated to be within 0.125 K for temperature, 0.05% for pressure, and 0.1% for the power, W_{net}.

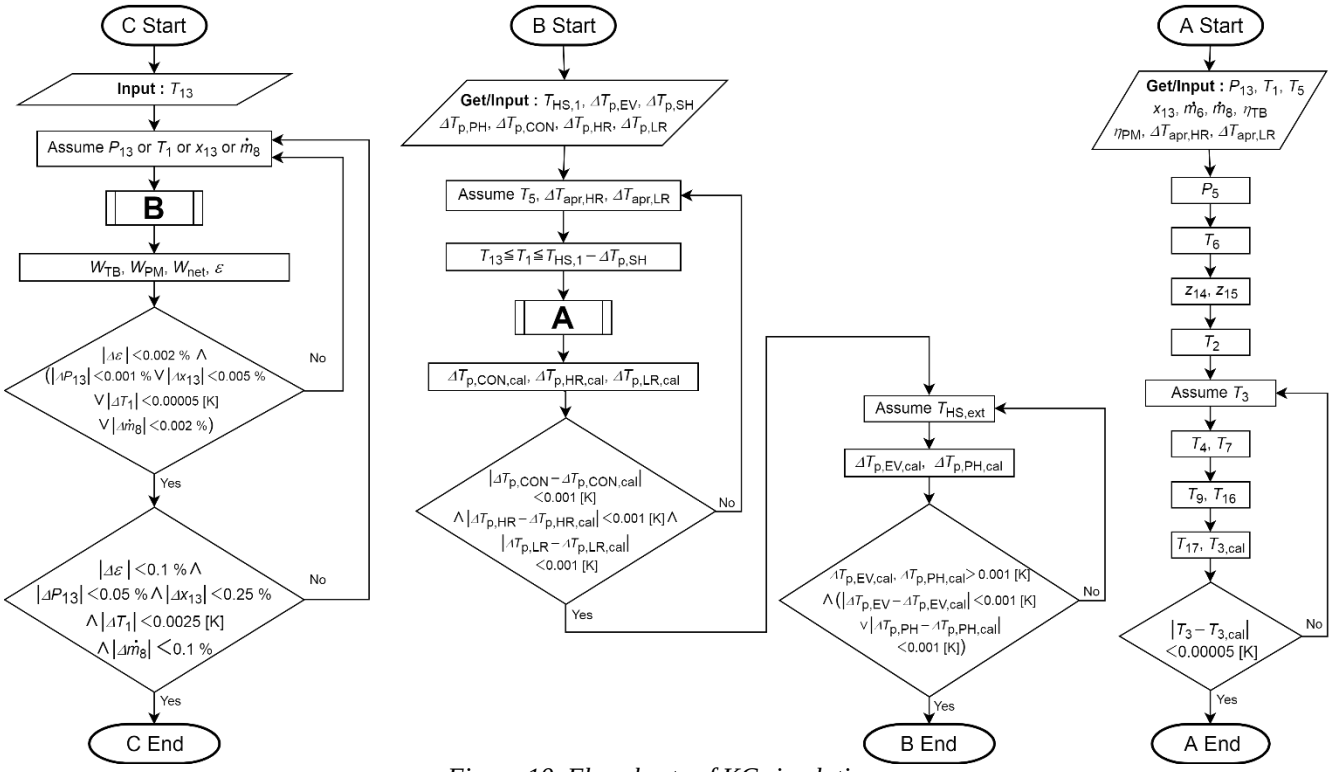

Figure 10. Flowcharts of KC simulation.

Table 5 shows the optimized parameters corresponding to the cycle configurations. Only the single-cycle arrangement ($n = 1$) is considered in the KC investigation, because the effectiveness of the multicycle is anticipated to be considerably reduced in cycles with a non-isothermal heating process [4].

3.4.2 Validation

The thermodynamic model of the KC in this study is compared with that proposed by Sun et al. [25]. The input parameters are shown in Table 6. Table 7 compares the results; as shown, the model in this study agrees well with Sun's model.

Table 5. Optimized parameters for KC.

Configuration	LR	HR arrangement	Optimized parameters	x_{13}	$\frac{\dot{m}_8}{\dot{m}_6}$
MRC	OFF	No	P_1, T_1	1	-
MRC-R	ON				-
KC-S	OFF	Series	P_1, T_1, T_{13}	-	1
KC-S-R	ON			-	
KC-P	OFF	Parallel	P_1, T_1, T_{13},	-	-
KC-P-R	ON		$\dot{m}_8$	-	-

Table 6. Input parameters for KC validation.

Item	Value	Item	Value
Case	K-1	$T_{CS,2}$ [°C]	10.91
P_1 [MPa]	2.354	η_{TB}	0.85
T_1 [°C]	130.5	η_{PM}	0.75
T_{13} [°C]	62.46	$\Delta T_{p,EV}$ [K]	0
z_6 [$_{NH3}$kg/kg]	0.9	$\Delta T_{p,CON}$ [K]	2.988
$T_{HS,1}$ [°C]	140	$\Delta T_{p,HR}$ [K]	0.728
$T_{HS,ext}$ [°C]	49.01	$\Delta T_{p,LR}$ [K]	140
$T_{CS,1}$ [°C]	4.5	$\Delta T_{p,SH}$ [K]	0

Table 7. Operating conditions in (a) Sun [25] and (b) this study.

Point	T [°C]		P [MPa]		z [$_{NH3}$kg/kg]		$\dot{m}/\dot{m}_6$	
No.	**(a)**	**(b)**	**(a)**	**(b)**	**(a)**	**(b)**	**(a)**	**(b)**
1	130.5	130.5	2.354	2.354	0.9991	0.9991	0.3181	0.3182
2	35.83	35.83	0.604	0.604	0.9	0.9	0.3181	0.3182
3-4	13.89	13.89	0.604	0.604	0.9	0.9	1	1
5	12.26	12.26	0.604	0.604	0.9	0.9	1	1
6-8	12.78	12.78	2.354	2.354	0.9	0.9	1	1
9, 12	46.42	46.42	2.354	2.354	0.9	0.9	1	1
13	62.46	62.46	2.354	2.354	0.9	0.9	1	1
14	62.46	62.46	2.354	2.354	0.9991	0.9991	0.3181	0.3182
15	62.46	62.46	2.354	2.354	0.8538	0.8537	0.6819	0.6818
16	13.51	13.50	2.354	2.354	0.8538	0.8537	0.6819	0.6818
17	13.76	13.76	0.604	0.604	0.8538	0.8537	0.6819	0.6818

3.4.3 Effect of CS Temperature

The effect of CS temperature is investigated for the AWMRC. The input conditions for the investigation are shown in Table 8. Figure 11 shows the results of the calculations, i.e., (a) the results when the CS temperature is a constant at 25 °C (cases M-1-1 and MR-1-1 in Table 8), and (b) those when the CS temperature changes from 30 °C (inlet) to 35 °C (outlet). Additionally, the results of the ARC under the same conditions are indicated in the figures for comparison.

Under the condition of constant CS temperature and the configuration without the LR (solid line in Figure 11(a)), the exergy efficiency, ε, increases with the EV inlet mass fraction, z_6, in the range above 0.6 $_{NH3}$kg/kg, and the ARC indicates the highest ε. Conversely, under the condition with the CS temperature gradient and the configuration without the LR (solid line in Figure 11(b)), ε becomes the highest at the EV inlet mass fraction of 0.98 $_{NH3}$kg/kg and 4.1% higher than that of ARC.

Under the condition of the CS temperature gradient (Figure 11(b)), the configuration with the LR (red broken line) indicates a 6.6% higher ε than that without the LR, and

2.0% higher under the condition of constant CS temperature (Figure 11(a)). The results indicate that the non-isothermal characteristic of the AWM is very effective for temperature-profile matching in both the cooling and heating processes.

Table 8. Input conditions for AWMRC with/without temperature gradient of CS.

Case	M-1-1	M-1-2	MR-1-1	MR-1-2
LR	OFF		ON	
$T_{CS,1}$ [°C]	25	30	25	30
$T_{CS,2}$ [°C]	25	35	25	35
z_6 [$_{NH3}$kg/kg]	0.3-0.99 (0.01 step)			
$T_{HS,1}$ [°C]	150			
$T_{HS,ext}$ [°C]	25			

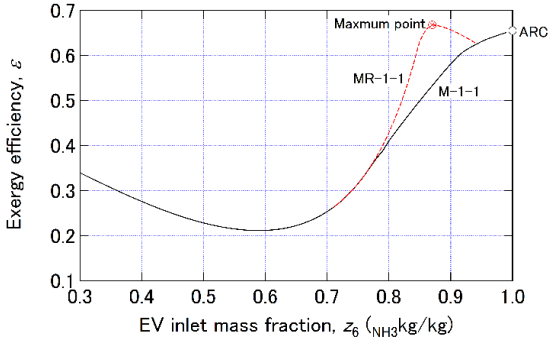

(a) Constant CS temperature

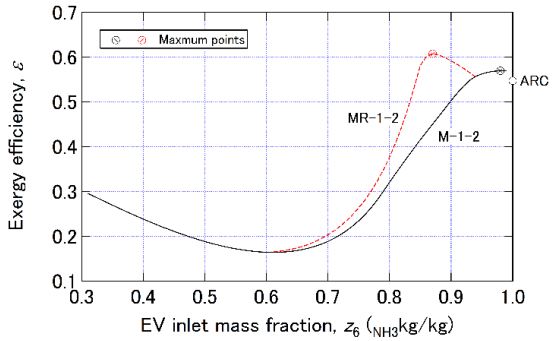

(b) Results with temperature gradient

Figure 11. Effect of CS temperature.

Therefore, the CS temperature conditions of 30 °C inlet and 35 °C outlet are considered in the KC investigation hereinafter.

3.4.4 Effect of Cycle-1 Inlet HS Temperature

The effect of the SH inlet HS temperature is investigated for six configuration patterns of the KC. The input conditions for the investigation are shown in Table 9. Figure 12 shows the calculation results, i.e., (a) bubbling temperature, T_B, of the AWM at the evaporating pressure, P_6, and EV inlet mass fraction, z_6, and (b) exergy efficiency, ε. The thin and thick colored lines correspond to the cycles with and without LR, respectively, and the loose broken black lines indicate CCE.

Table 9. Input conditions for KC simulations.

Case	M-2	KS-2	KP-2	MR-2	KSR-2	KPR-2
Configuration♣	MRC	KC-S	KC-P	MRC-R	KC-S-R	KC-P-R
z_6 [$_{NH3}$kg/kg]	0.3-0.99 (0.01 step)			0.3-0.95 (0.01 step)		
$T_{CS,1}$ [°C]	30					
$T_{CS,2}$ [°C]	35					
$T_{HS,1}$ [°C]	100-175 (25-K-step)					
$T_{HS,ext}$ [°C]	25					

♣Table 7

The findings indicate that the temperature, T_B, in the cycles without the LR demonstrates effective agreement with the estimation, while those of the cycles with the LR are lower than the estimated values by approximately 10 K. The temperature–entropy (T–S) diagrams of the AWMRC with and without the LR at the 150 °C SH inlet HS temperature, $T_{HS,1}$, are shown in Figure 13 (configurations of (a) MRC and (b) MRC-R in Table 7, respectively). The blue dashed line squares correspond to the CCs obtained by the CC model. Figure 13(a) reveals that a major part of the areas enclosed by the T–S diagrams of the AWMRC and the corresponding CC overlap each other, and the difference between T_B and the high-temperature of the corresponding CC is 2.60 K.

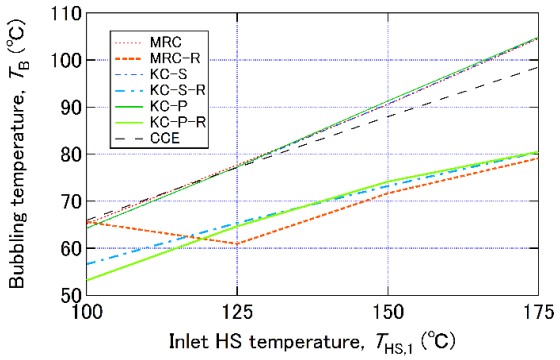

(a) Bubbling temperature

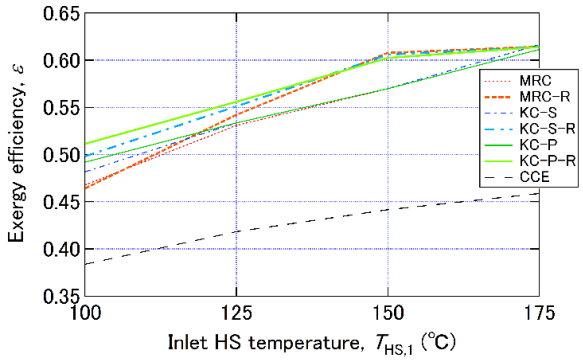

(b) Exergy efficiency

Figure 12. Effect of cycle-1 inlet HS temperature on KC.

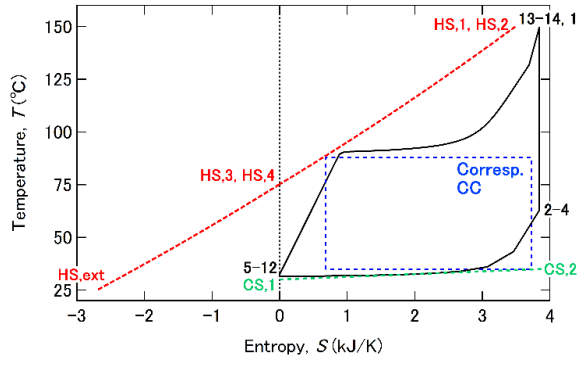

(a) AWMRC

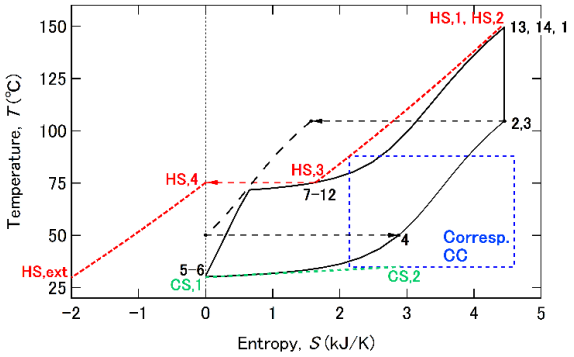

(b) AWMRC+LR

Figure 13. Temperature–entropy diagrams of AWMRC.

Figure 13(b) shows that the cycle with the LR involves a lower T_{B} such that the steep temperature-changing part of the evaporation process matches the HS temperature change. Consequently, T_{B} becomes approximately 10 K lower than the estimated value.

Figure 12(b) shows that the appropriate configuration changes by $T_{\mathrm{HS},1}$. At 100 °C, the configuration KC-P-R indicates the highest ε. At 150 °C, the efficiencies, ε, of the three configurations with the LR are approximately equal and become the highest; therefore, the configuration MRC-R is adequate. At 175 °C, the efficiencies, ε, of all configurations are approximately equal; therefore, the configuration MRC becomes feasible. The findings indicate that the KC is effective in the range below 125 °C, and the LR is the most effective at 150 °C HS temperature and loses the advantage at 175 °C.

3.5. Practical Scenarios

The analysis and the models in this study are assumed ideal conditions. They should be approached to more practical conditions such as lower turbine and pump efficiencies, and pressure loss are considered. The analysis will be extended with additional consideration of irreversibility on heat-transfer, expansion and compression processes.

4. Conclusions

This paper presented a condition that produces maximal power from a single constant-heat HS with a finite number of thermodynamic cycles.

First, a model that assumed a succession of finite number of CCs under constant-specific-heat heat sources was analyzed. The conditions for obtaining maximal power with respect to the inlet/outlet HS temperature were derived analytically. The analysis also showed the relation between the number of the cycles and exergy efficiency, and the number should be selected as it satisfies the required exergy efficiency.

Next, the model was compared to the optimized ARC. It was confirmed that the RCs and the estimation by the CCs exhibited similar trends in terms of evaporating temperatures and exergy efficiency. The difference between the RC's evaporating temperature, $T_{5,i}$, and estimated temperature decreased in the higher-temperature cycle. The differences in the temperature, $T_{5,i}$, of the lower-temperature RC and in the exergy efficiency increased with the cycle-1 inlet HS temperature, $T_{\mathrm{HS},1,1}$.

Finally, the optimized six-configuration patterns of the KC (including AWMRC) were compared to those of the CC model. The bubbling temperatures, T_{B}, of the KC configurations without the LR demonstrated good agreement with the estimated temperatures, while those of the configurations with the LR became approximately 10 K lower than the estimation. The reasons for these were explained by *T*–*S* diagrams of the AWMRC with and without the LR. Additionally, the optimized results of the RC and KC were explained.

The comparisons demonstrated that the CC model provided an effective estimation of the temperature conditions for the heat-recovery cycles producing maximal power from a non-isothermal HS, especially for a single cycle without LR.

Using the proposed method, the required number of cycles and their operating conditions under a given heat source condition can be estimated, without any information about cycle configurations, types of working fluids, and iteration of simulation calculation under inappropriate conditions. In addition, a systematic exploration of the optimal system [26, 27] can be started from the proper initial condition.

The analysis will be extended with additional consideration of irreversibility on heat-transfer, expansion and compression processes.

Acknowledgments

Conflicts of interest: none. We would like to thank Editage (www.editage.com) for English language editing.

Nomenclature

c	specific heat [kJ/(kg K)]
e	specific exergy [kJ/kg]
i	cycle number
j	parameter for sigma
$\dot{m}$	mass flow rate [kg/s]
n	number of cycles
P	pressure [MPa]
$\dot{Q}$	heating rate [kW]
S	entropy [kJ/(kg K)]
T	temperature [°C]
W	power [kW]
x	dryness fraction [kg(dry vapor)/kg]
z	ammonia mass fraction [$_{\mathrm{NH3}}$kg/kg]

Greek symbols

α, β, γ,	algebra for Eq.(3) results
Δ	differences between a loop and the 1-time previous loop
ΔT_{a}	minimum temperature difference between CC and HS [K]
ΔT_{b}	minimum temperature difference between CC and CS [K]
ΔT_{p}	pinch temperature [K]
ε	exergy efficiency
η	efficiency

Subscripts, superscripts, and abbreviations

0	ambient
1, 2, 3, …	cycle No. (CC model and RC) /point No. (see Figures 4 and 5)
apr	approach temperature
ARC	ammonia Rankine cycle
AWM	ammonia-water mixture
AWMRC	ammonia-water mixture Rankine cycle
B	bubbling, saturated liquid
cal	calculated
CC	Carnot cycle
CCE	estimation by Carnot cycle model
CON	condenser
CS	cold source
D	dewing, saturated vapor

EV	evaporator
ext	exit
h	high-temperature of Carnot cycle
HR	high-temperature recuperator
HS	hot source
KC	Kalina cycle
l	low-temperature of Carnot cycle
LR	low-temperature recuperator
net	net
PH	preheater
PM	pump
RC	Rankine cycle
SH	superheater
sum	sum of net powers
TB	turbine
thm	thermal efficiency

References

[1] X. Zhang, M. He, Y. Zhang, "A review of research on the Kalina cycle," *Renew. Sustain. Energy Rev., 16*, 5309-5318, 2012. doi: 10.1016/j.rser.2012.05.040.

[2] M. Fallah, S. Mohammad S. Mahmoudi, M. Yari, R. A. Ghiasi, "Advanced exergy analysis of the Kalina cycle applied for low temperature enhanced geothermal system," *Energy Convers. Manag*, *50*, 576-582, 2009.

[3] J. Bao, L. Zhao, "A review of working fluid and expander selections for organic Rankine cycle," *Renew. Sustain. Energy Rev.*, *24*, 325-342, 2013. doi: 10.1016/j.rser.2013.03.040

[4] D. Walraven, B. Laenen, W. D'haeseleer, "Comparison of thermodynamic cycles for power production from low-temperature geothermal heat sources," *Energy Convers. Manag.*, *66*, 220-233, 2013. doi: 10.1016/j.enconman.2012.10.003.

[5] P. Bombarda, C. M. Invernizzi, C. Pietra, "Heat recovery from Diesel engines: A thermodynamic comparison between Kalina and ORC cycles," *Appl. Therm. Eng.*, *30*, 212-219, 2012. doi: 10.1016/j.applthermaleng.2009.08.006.

[6] V. Zare, S. M. S. Mahmoudi, "A thermodynamic comparison between organic Rankine and Kalina cycles for waste heat recovery from the Gas Turbine-Modular Helium Reactor," *Energy*, *79*, 398-406, 2015. doi: 10.1016/j.energy.2014.11.026.

[7] Y. Dai, J. Wang, L. Gao, "Parametric optimization and comparative study of organic Rankine cycle (ORC) for low grade waste heat recovery," *Energy Convers. Manag.*, *50*, 576-582, 2009. doi: 10.1016/j.enconman.2008.10.018.

[8] S. Aphornratana, I.W. Eames, "Thermodynamic analysis of absorption refrigeration cycles using the second law of thermodynamics method," *Int. J. Refrig.*, *18*, 244-252, 1995. doi: 10.1016/0140-7007(95)00007-X.

[9] J. P. Roy, M. K. Mishra, A. Misra, "Parametric optimization and performance analysis of a waste heat recovery system using Organic Rankine Cycle," *Energy*, *35*, 5049-5062, 2010. doi: 10.1016/j.energy.2010.08.013.

[10] A. M. Delgado-Torres, L. García-Rodríguez, "Analysis and optimization of the low-temperature solar organic Rankine cycle (ORC)," *Energy Convers. Manag.*, *51*, 2846-2856, 2010. doi: 10.1016/j.enconman.2010.06.022.

[11] Z. Q. Wang, N. J. Zhou, J. Guo, X. Y. Wang, "Fluid selection and parametric optimization of organic Rankine cycle using low temperature waste heat," *Energy*, *40*, 107-115, 2012. doi: 10.1016/j.energy.2012.02.022.

[12] T. C. Hung, S. K. Wang, C. H. Kuo, B. S. Pei, K. F. Tsai, "A study of organic working fluids on system efficiency of an ORC using low-grade energy sources," *Energy*, *35*, 1403-1411, 2010. doi: 10.1016/j.energy.2009.11.025.

[13] A. I. Papadopoulos, M. Stijepovic, P. Linke, "On the systematic design and selection of optimal working fluids for Organic Rankine Cycles," *Appl. Therm. Eng.*, *30*, 760-769, 2010. doi: 10.1016/j.applthermaleng.2009.12.006.

[14] H. D. M. Hettiarachchi, M. Golubovic, W. M. Worek, Y. Ikegami, "The performance of the Kalina cycle system 11(KCS-11) with low-temperature heat sources," *J. Energy Resour. Technol.*, *129*, 243-247, 2007. doi: 10.1115/1.2748815.

[15] S. Ogriseck, "Integration of Kalina cycle in a combined heat and power plant, a case study," *Appl. Therm. Eng.*, *29*, 2843-2848, 2009. doi: 10.1016/j.applthermaleng.2009.02.006.

[16] H. Saffari, S. Sadeghi, M. Khoshzat, P. Mehregan, "Thermodynamic analysis and optimization of a geothermal Kalina cycle system using Artificial Bee Colony algorithm," *Renew. Energy*, *89*, 154-167, 2016. doi: 10.1016/j.renene.2015.11.087.

[17] O. K. Singh, S. C. Kaushik, "Energy and exergy analysis and optimization of Kalina cycle coupled with a coal fired steam power plant," *Appl. Therm. Eng.*, *29*, 2843-2848, 2009. doi: 10.1016/j.applthermaleng.2012.10.006.

[18] R. Bahrampoury, A. Behbahaninia, "Thermodynamic optimization and thermoeconomic analysis of four double pressure Kalina cycles driven from Kalina cycle system 11," *Energy Convers. Manag*, *152*, 110-123, 2017. doi: 10.1016/j.enconman.2017.09.046.

[19] A. Bejan, *Entropy generation minimization: The method of thermodynamic optimization of finite-size systems and finite-time processes*, New York, USA: CRC Press, 1995.

[20] F. L. Curzon, B. Ahlborn "Efficiency of a Carnot engine at maximum power output," *Am. J. Phys.*, *43*, 22-24, 1975. doi: 10.1119/1.10023.

[21] A. Bejan, M. R. Errera, "Maximum power from a hot stream," *Int. J. Heat Mass Transf.*, *41*, 2025-2035, 1998. doi:10.1016/S0017-9310(97)00256-1.

[22] PROPATH Group, *PROPATH: A Program package for thermophysical properties, version 13.1*, 2008.

[23] R. Tillner-Roth, F. Harms-Watzenberg, H. D. Baehr, "Eine neue Fundamentalgleichung fur Ammoniak," *DKV-Tagungsbericht*, *20*, 167-181, 1993.

[24] O. M. Ibrahim, S. A. Klein, "Thermodynamic properties of ammonia-water mixtures," *ASHRAE Trans.*, *99*, 1495-1502, 1993.

[25] F. Sun, W. Zhou, Y. Ikegami, K. Nakagami, X. Su, "Energy–exergy analysis and optimization of the solar-boosted Kalina cycle system 11 (KCS-11)," *Renew. Energy*, *66*, 268-279, 2014.doi: 10.1016/j.renene.2013.12.015.

[26] A. Toffolo, S. Rech, A. Lazzaretto, "Generation of Complex Energy Systems by Combination of Elementary Processes," *J. Energy Resour. Technol.*, *140*, 1-11, 2018. doi: 10.1115/1.4040194.

[27] K. Seki, K. Takeshita, Y. Amano, "Development of Complex Energy Systems with Absorption Technology by Combining Elementary Processes," *Energies*, *12*, 495, 2019. doi: 10.1016/10.3390/en12030495.